



Cite this: *J. Anal. At. Spectrom.*, 2024, **39**, 1388

Quantification capabilities of N₂ MICAP-MS with solution nebulization and aerosol desolvation†

Monique Kuonen,  Bodo Hattendorf  and Detlef Günther *

The analytical capabilities of a nitrogen-sustained high-power microwave inductively coupled atmospheric-pressure plasma mass spectrometer (N₂ MICAP-MS) were investigated using solution nebulization with and without aerosol desolvation. The reduced solvent load for the desolvated aerosol and the increased aerosol transfer resulted in a signal enhancement of ten times for most elements in samples without a significant amount of dissolved solids. An exception was boron, whose signal decreased by a factor of seven when a desolvator was used. To compare the accuracy, reproducibility, and matrix susceptibility of the N₂ MICAP-MS, the mass fractions of 30 elements were determined in two certified water reference materials using external calibration and standard addition. The results were generally found to agree within 10% of the certified reference values with a maximum deviation of 17% in the case of ⁶⁴Zn. Comparing external calibration and standard addition provided comparable results regardless of the sample introduction method. To assess the extent of matrix effects, multi-element standard solutions were doped with amounts of up to 100 mg kg⁻¹ calcium. This resulted in a signal suppression of up to 30% and 70% for conventional nebulization and aerosol desolvation, respectively. This substantially reduced the improvement in sensitivity observed for the desolvated aerosol. To further investigate the fundamental characteristics of the N₂ MICAP-MS, the plasma gas temperature was estimated using three methods. The determined temperatures for the two most reliable methods were in the range of ~5000–6000 K and were found to be independent of the sample introduction method and similar to those of an Ar ICP.

Received 16th February 2024
 Accepted 21st March 2024

DOI: 10.1039/d4ja00058g

rsc.li/jaas

Introduction

In recent years, there has been a renewed interest in nitrogen-sustained microwave-induced plasmas (MIPs) for both optical emission spectroscopy (OES) and mass spectrometry (MS) due to the introduction of the microwave inductively coupled atmospheric-pressure plasma (MICAP).¹ While several MIPs were investigated as an alternative ion source, early designs were limited by their low operating power.^{2–4} The first high-power nitrogen MIP was based on an Okamoto cavity⁵ and after its successful coupling to MS,⁶ commercial instruments were developed by Hitachi. However, these high-power N₂ MIP-MS were only sold in Japan⁷ and have thus not been widely distributed.⁸ The emerging MICAP is another high-power nitrogen plasma that can be used as an alternative ion source for OES⁹ and MS.¹⁰ Compared to the conventional argon-based inductively coupled plasma (ICP) employed for these analytical techniques,^{11–13} the nitrogen microwave plasmas are more cost-effective in their operation and reduce the occurrence of argon-

containing spectral interferences.^{6,14} In addition, the MICAP should exhibit a negligible plasma potential since the microwave coupling is purely inductive. Its plasma geometry is essentially identical to that of an Ar ICP because it is created in a conventional Fassel-type torch.¹ Due to all these similarities, the MICAP can be used with all existing sample introduction methods available for ICP-MS.

For conventional ICP-MS, the argon-based plasma background ions can interfere with several isotopes.¹⁵ For example, the plasma species ³⁸Ar¹H⁺, ⁴⁰Ar⁺, ⁴⁰Ar¹²C⁺, ⁴⁰Ar¹⁶O⁺, and ⁴⁰Ar₂⁺ interfere with the most abundant isotopes of potassium, calcium, chromium, iron, and selenium. Other argides can be formed with abundant elements, resulting in polyatomic ions such as ⁴⁰Ar³⁵Cl⁺ and ⁴⁰Ar²³Na⁺, which interfere with arsenic and the major isotope of copper. Traditionally, these spectral interferences can be decreased or resolved by using reaction or collision cells^{16–18} or instruments with higher mass resolution.¹⁹ Replacing an argon with a nitrogen plasma is another way to reduce these interfering species. However, with a nitrogen-sustained plasma, the occurrence of nitrogen-based plasma species and nitrides of matrix elements increases. The most abundant spectral interferences are caused by ¹⁴N_x¹⁶O_y⁺ (x = 1–4, y = 0–2) and directly affect the detection of silicon, phosphorous, calcium, titanium, iron, and nickel, although not

Department of Chemistry and Applied Biosciences, Laboratory of Inorganic Chemistry, ETH Zurich, Vladimir-Prelog-Weg 1, 8093, Zurich, Switzerland. E-mail: guenther@inorg.chem.ethz.ch

† Electronic supplementary information (ESI) available. See DOI: <https://doi.org/10.1039/d4ja00058g>



always their main isotope.^{6,10,20} In addition to oxides, the occurrence of nitride adduct ions needs to be considered due to the high abundance of nitrogen. However, since most interferences in an argon plasma occur at different m/z than those occurring in a nitrogen plasma, different elements and isotopes are affected.

Early MIPs such as the Beenakker cavity,² the Surfatron,³ and the microwave plasma torch⁴ had lower matrix and mass load tolerance, which is often presumed to apply to all MIPs. However, similar to other high-power MIPs like the Okamoto⁵ and Hammer²¹ cavities, the MICAP can handle the mass load from conventional liquid sample introduction such as solution nebulization. Furthermore, the N₂ MICAP has demonstrated a high solvent tolerance, as it was stable even when introducing organic solvents.⁹ Although there are only a few publications on the matrix tolerance of the N₂ sustained MICAP, they differ in the reported severity of the matrix effects. While studies with OES detection reported significant signal suppression on ionic emission lines,^{9,22,23} the matrix tolerance for MS was described to be similar to that of an Ar ICP.^{10,24} Regardless of the employed analytical technique (OES, MS), further investigations are needed to characterize the MICAP matrix and mass load tolerance.

The solvent load of the sample introduced into the plasma can be reduced by using aerosol desolvation. This leads to a decrease in the energy required for the solvent vapor to dissociate^{25,26} and lowers the occurrence of solvent-based interferences.^{27,28} In addition to a reduced solvent load, aerosol desolvation results in a higher aerosol yield due to an increased nebulization respectively transport efficiency. While aerosol desolvation has been shown to increase the analyte signal in an Ar ICP-MS,^{25–28} some analytes can be lost in the desolvation unit.^{28–30} So far, only Schild *et al.*¹⁰ used a desolvation system to investigate the performance of an N₂ MICAP-TOFMS and observed a five to ten-fold analyte signal increase.

Recent experiments using a nitrogen plasma,^{9,10,22–24,31,32} including the first successful quantification studies with ion chromatography,³³ laser ablation,²⁰ or solution nebulization³⁴ have indicated that the MICAP can be a very promising alternative to the Ar ICP as ion source. The latter quantified heavy metals in digested soil samples with MS but was limited to only nine isotopes (⁵¹V, ⁵³Cr, ⁵⁹Co, ⁶²Ni, ⁶⁵Cu, ⁶⁶Zn, ⁷⁵As, ¹¹²Cd, ²⁰⁷Pb).³⁴ This study is focused on the characterization of the nitrogen-sustained MICAP quadrupole MS for the multielement analysis of aqueous solutions, which is a routine application of Ar ICP-MS. Two water reference materials were used to investigate the quantification capabilities using conventional solution nebulization (SN) and aerosol desolvation (Des). The reference materials were quantified by external calibration as well as standard addition to assess the effects of signal suppression. Both sample introduction methods were employed to compare figures of merit such as trueness, precision, and limits of detection. Furthermore, to compare the N₂ MICAP-MS with an Ar-based ICP-MS, the gas kinetic temperature was determined for both introduction methods using the pressure reduction in the interface region³⁵ or the formation of singly charged monoxide rare earth elements and their known dissociation energies.^{36,37}

Experimental

Instrumentation

The employed prototype has already been described in an earlier publication with more detail.³¹ In short, the nitrogen-sustained MICAP ion source (Radom Corp., USA) was coupled to an ELAN 6100 DRC quadrupole mass spectrometer (PerkinElmer/Sciex, Canada). Additionally, a pressure sensor (CMR 632, Pfeiffer, DE) was connected to the interface vacuum line to measure the interface pressure. The plasma can be ignited and controlled through the MICAP control unit and software, while the mass spectrometer is operated through the ELAN software. The liquid samples were introduced by pneumatic nebulization using a MicroMist™ glass concentric nebulizer (Glass Expansion, AUS) with a cyclonic spray chamber or inserted in an Apex-Q system (Elemental Scientific, USA) for aerosol desolvation. The sample flow rate was controlled with a peristaltic pump, adjusted to 1.37 mL min⁻¹ for solution nebulization and 0.84 mL min⁻¹ for desolvated sample introduction.

Materials and methods

The instrument was optimized while aspirating a multi-element solution containing 1 µg kg⁻¹ Li, Be, Na, Mg, K, Ca, Co, Zn, Ge, As, Se, Rb, Sr, Cd, In, Cs, Te, Ba, Ce, Lu, Pb, Th, U, which was prepared by diluting single-element stock solutions from Merck, Inorganic Ventures and VWR chemicals. The optimization for solution nebulization was performed by optimizing for maximum ²³⁸U⁺ signal intensity at a magnetron power of 1450 W and a nebulizer gas flow rate that maintained a ¹⁴⁰Ce¹⁶O⁺/¹⁴⁰Ce⁺ formation rate below 3%. When using aerosol desolvation, the instrument was also optimized for maximum ²³⁸U⁺ signal intensity while keeping the cerium oxide level below 1%. Due to the lower ¹⁴⁰Ce¹⁶O⁺ abundance, aerosol desolvation allowed the use of higher nebulizer gas flow rates. An overview of the operating conditions is given in Table 1.

Two water reference materials were selected for this study. The river water SLRS-6 (National Research Council Canada, NRCC), is certified for 20 elements, ranging from 0.006 µg kg⁻¹–8800 µg kg⁻¹, and the SRM 1643f (National Institute of Standards and Technology, NIST), which is certified for 29 elements with

Table 1 Typical N₂ MICAP-MS operating parameters with solution nebulization (SN) and aerosol desolvation (Des) as sample introduction for quantitative analyses. An ion lens calibration was carried out for both operating conditions

Parameter	Value
Cooling gas flow rate	14 L min ⁻¹
Auxiliary gas flow rate	750 mL min ⁻¹
Nebulizer gas flow rate	SN: 900 mL min ⁻¹ , Des: 1000 mL min ⁻¹
Magnetron power	1450 W
Sampler cone	1.1 mm Ø, Pt
Skimmer cone	0.8 mm Ø, Pt
Quadrupole rod offset	-5 V
Cell rod offset	-10 V
Call path voltage	-50 V
Spray chamber temperature	SN: room temperature, Des: 140 °C
Condenser	SN: none, Des: 2 °C



mass fractions between $0.96 \mu\text{g kg}^{-1}$ – $29\,000 \mu\text{g kg}^{-1}$ (Fig. S1†). In both samples, Ca, Na, Mg, and K are the most abundant elements. Since NIST 1643f has higher concentrations but is otherwise similar to SLRS-6, a multi-element stock solution with similar analyte ratios as in the two (NIST 1643f and SLRS-6) reference solutions was prepared (see Table S1†). For the analysis, the river water SLRS-6 was diluted by a factor of 2 with 1% (v/v) nitric acid, while the NIST 1643f sample was diluted once by a factor of 2 and once by a factor of 10. Using the multi-element stock solution seven calibration solutions were prepared to cover the concentration range of the analytes in the reference samples for the external calibration. For the standard addition, multi-element solutions with a similar concentration to the corresponding reference sample but without the matrix elements were added to two aliquots of the reference samples. Indium was added to all solutions (samples, external calibrations, standard additions) at a concentration of $5 \mu\text{g kg}^{-1}$ as an internal standard. At least one isotope per element was measured with a dwell time of 500 ms using one sweep and 5 replicates.

Previous reports have indicated that the N_2 MICAP-MS has a similar matrix tolerance as a conventional Ar ICP-MS.^{10,24} Since Ca is the major matrix element in the investigated reference samples, the influence of an elevated calcium concentration on the analyte signal was studied. Therefore, five solutions with 1–100 mg kg^{-1} calcium (as nitrate) were prepared and analyzed using two different sample introduction systems (SN and Des). Each solution contained a 1000-fold dilution of the multi-element standard VI (Merck, Germany) and a total of $300 \mu\text{g kg}^{-1}$ boron.

Plasma gas temperatures were estimated using three different methods. The first is based on the pressure reduction in the interface when the plasma is sampled relative to the pressure at room temperature with the interface pump and the gas flows on.³⁵ The other two methods are based on the abundance ratios of metal-oxide ions to the metal ions (MO^+/M^+) and their known dissociation energies. According to Longerich,³⁶ the temperature can be estimated from the mass-bias corrected rare earth element (REE) oxide abundance ratios and their known dissociation energies with a linear regression.³⁸ This method however appeared to overestimate the temperatures for an Ar plasma substantially when compared to other Boltzmann plot methods.^{39,40} Houk and Praphairaksit (abbr. as H&P)³⁷ on the other hand suggested estimating the gas temperature from these abundance ratios *via* statistical thermodynamics, including partition functions and spectroscopic constants of the corresponding species.

Single element REE solutions of $100 \mu\text{g kg}^{-1}$ La, Ce, Pr, Eu, Tb, Ho, Tm, and Lu were prepared from stock solutions (Inorganic Ventures, USA) in 1% (v/v) nitric acid and contained $10 \mu\text{g kg}^{-1}$ Rh as internal standard. Each isotope was measured for

500 ms in one sweep with 5 replicates. The mass discrimination was determined from the molar sensitivities of the REE isotopes. The oxygen density in the central channel of the plasma was estimated from the solution flux (as H_2O) reaching the ion source. This was determined from the difference in solution uptake and spray chamber drain. The measurements were carried out with and without aerosol desolvation using the N_2 MICAP-MS and an Ar-based ICP-MS (Elan 6100 DRCII, PerkinElmer/Sciex, Canada) for comparison.

Data evaluation

Element mass fractions were determined from the blank-corrected signal intensities while taking the blank-corrected signal of the internal standard and the dilution factor into account. The uncertainties of the results were estimated from the relative standard deviation of the corresponding reference samples. Limits of quantification (LOQs) were obtained from ten times the standard deviation of the blank divided by the slope of the calibration curve. Furthermore, limits of detection (LODs) were determined from three times the standard deviation of the blank divided by the elements' blank-corrected sensitivities.

The temperature in the ICP region was calculated with the pressure reduction method, which is based on the correlation of pressure and temperature:³⁵

$$\frac{T_{\text{plasma}}}{T_{\text{room}}} = \left(\frac{P_{\text{interface}}}{P_{\text{plasma}}} \right)^2 \quad (1)$$

where T_{plasma} is the gas temperature of the plasma source, T_{room} the room temperature (300 K), $P_{\text{interface}}$ the pressure in the interface with the plasma off but interface pump and gas flows on, and P_{plasma} the interface pressure when the plasma is stable. The temperature was also determined according to Longerich³⁶ by using different REEs and their oxides with their dissociation energies. A linear regression was performed according to the relationship given by:

$$\log\left(\frac{[\text{MO}^+]}{[\text{M}^+]}\right) = \frac{D_{\text{E}}}{R \times \ln(10) \times T_{\text{plasma}}} + q \quad (2)$$

with $[\text{M}^+]$ and $[\text{MO}^+]$ being the measured, mass-bias corrected intensities of atomic and oxide ions, D_{E} the dissociation energy of the oxide ion, R the universal gas constant, and q a constant term. The linear relationship between the logarithm of the metal-oxide ion to metal ion abundance ratios and the dissociation energies D_{E} can be employed to calculate the plasma temperature T_{plasma} from the slope of the regression.

The third method to calculate the plasma temperature is based on the expression of the dissociation constant from statistical thermodynamics:³⁷

$$\begin{aligned} \log\left(\frac{[\text{M}^+] \times n_{\text{O}}}{[\text{MO}^+]}\right) &= \frac{1}{2} \log(T_{\text{plasma}}) - \frac{5040 D_{\text{E}}}{T_{\text{plasma}}} + \frac{3}{2} \log\left(\frac{M_{\text{M}^+} M_{\text{O}}}{M_{\text{MO}^+}}\right) - \log(g) \\ &+ \log\left(\frac{z_{\text{elec}}^{\text{M}^+} z_{\text{elec}}^{\text{O}}}{z_{\text{elec}}^{\text{MO}^+}}\right) + \log(B) + \log\left(1 - 10^{-0.625\omega/T_{\text{plasma}}}\right) + 20.432 \end{aligned} \quad (3)$$



in this equation, the measured, mass-bias corrected intensity ratio $[M^+]/[MO^+]$ is used as a proxy for their density ratio. The density of the neutral oxygen n_O in cm^{-3} was estimated from the introduced water.⁴¹ T_{plasma} is the unknown plasma gas temperature in K, D_E the dissociation energy in eV, while M_M , M_O , and M_{MO} are the atomic or molecular masses of the involved species in g mol^{-1} . The vibrational and rotational constants of the metal-oxide ions ω and B are in cm^{-1} . z_{elec} denotes the electronic partition functions, which for the molecule is assumed to be equal to the statistical weight g of the ground electronic state. The constant at the end of the equation is a collection of independent numerical values and is only true for a heteronuclear diatomic molecule.³⁷ To estimate T_{plasma} using this equation, an iterative approach is required. The values for the dissociation energy and the spectroscopic constants were taken from the original paper,³⁷ while the electronic partition functions were calculated from the NIST database.⁴² The density of oxygen was estimated from the water flux into the central channel of the plasma.

Results and discussion

Influence of aerosol desolvation

Experiments were performed to study if the signal enhancement observed with aerosol desolvation¹⁰ is primarily due to a reduced solvent load or an increased aerosol transfer to the ICP. To separate the two processes, the aerosol of the externally mounted spray chamber was guided through the Apex-Q system, and measurements were carried out with and without active aerosol desolvation. Ion signals were measured for a suite of selected elements while the nebulizer gas flow rate was increased from 800 mL min^{-1} to 1000 mL min^{-1} . With aerosol desolvation, a five to ten times lower metal-oxide ratio was obtained.

Sensitivity ratios for the measured isotopes with relative to without aerosol desolvation are given in Table S2.† Elements with ionization energies below that of NO were only moderately affected by aerosol desolvation. Interestingly, however, there was a mass-dependent effect, with lighter isotopes showing slight enhancement for the desolvated aerosol at low nebulizer gas flow rates while isotopes above m/z 133 were suppressed to a similar extent (Fig. S2†). When increasing the gas flow rate, however, the enhancement for lighter isotopes gradually ceased and eventually a similar suppression was observed for all these isotopes. Elements with a high first ionization energy ($\text{IE} \geq 9 \text{ eV}$) such as Be, Zn, As, Se, Cd, and Te on the other hand exhibited remarkable enhancement with the desolvated aerosol, which is assumed to be caused by the lower abundance of NO in the ion source. NO has an ionization energy of (9.264 eV),³⁸ which is close to or below that of these elements. It is thus likely that lowering the abundance of NO in the plasma by reducing the water load (approx. 40% at 800 mL min^{-1}) increases the ion yield of these elements and overcompensates for the suppression observed for the other elements of similar mass. In general, however, it appears that aerosol desolvation alone only leads to a substantial change in the ion yield for elements with high IE, while other elements are only moderately affected. This

would indicate that the sensitivity enhancements frequently observed for aerosols produced with aerosol desolvation are primarily due to a higher transport efficiency of the elements from the nebulizer to the plasma and possibly a higher nebulization efficiency rather than by a change in plasma conditions.

Temperature determination

The plasma temperatures were determined for conventional solution nebulization and using the Apex-Q system with the nebulizer directly inserted into the heated spray chamber. The results for the three methods^{35–37} are summarized in Table 2 and compared to the temperatures of an Ar ICP with the same vacuum interface and MS configuration (Elan DRC II).

The gas temperature estimates obtained by the pressure reduction method showed similar values with and without aerosol desolvation but differed between the N_2 and Ar plasmas. The similar results for the introduction methods can be explained by the fact that they were estimated at the respective optimized conditions of the N_2 MICAP-MS. The higher nebulizer gas flow rate used with aerosol desolvation leads to a cooling of the plasma similar to the water vapor present without aerosol desolvation. Reducing the nebulizer gas flow rate with aerosol desolvation from 1000 mL min^{-1} to 900 mL min^{-1} resulted in higher temperature estimates (see Table S3†). Nonetheless, the results of the pressure reduction method suggest that the gas temperature of an Ar ICP is about $\sim 500 \text{ K}$ higher than that of the N_2 MICAP. This difference, however, may be due to a slightly lower oxide ratio (2.6% CeO^+ vs. 2.9% CeO^+) or the bigger pressure fluctuations that were observed when measuring the interface pressure with the plasma off. However, comparing the N_2 MICAP temperature estimates with reported values for an Ar ICP, which was determined to be $\sim 5000 \text{ K}$ by Fulford and Douglas³⁵ and 5280 K by Houk and Praphairaksit,³⁷ no substantial difference can be seen (Table 2). The temperatures obtained *via* the Longerich method³⁶ are higher than the other values, however, this method has always resulted in values between 9000 K and 13000 K . Using statistical thermodynamics, temperatures of $\sim 5900\text{--}6700 \text{ K}$ were obtained. These temperatures are similar

Table 2 Calculated plasma temperatures were obtained from the pressure reduction method, the Longerich method, and the method from Houk and Praphairaksit (H&P). Temperatures were calculated for solution nebulization (SN) and desolvated (Des) sample introduction for both the N_2 MICAP and the Ar ICP. The Ar ICP-MS was operated at 1450 W and 900 mL min^{-1} for SN and 1000 mL min^{-1} for Des the operating conditions of the N_2 MICAP-MS are listed in Table 1

Method	N_2 MICAP		Ar ICP	
	SN	Des	SN	Des
Pressure reduction	5220 K	5270 K	5780 K	5680 K
Longerich	12850 K	13800 K	13170 K	12600 K
H&P LaO^+/La^+	6350 K	6430 K	6620 K	6710 K
H&P CeO^+/Ce^+	5910 K	5980 K	6060 K	6250 K
H&P PrO^+/Pr^+	6200 K	6300 K	6080 K	6300 K



for both sample introduction methods and the difference between the N_2 and the Ar plasma is less than 300 K for the individual REEs. However, these differences are smaller than those between different REEs. This element dependency ($T_{La} > T_{Pr} > T_{Ce}$) and its magnitude has been previously reported by Houk and Praphairaksit³⁷ and is possibly a result of assumptions made within this model. The substantial differences between H&P and the pressure reduction method are assumed to be due to uncertainties in the oxygen density used in our experiments. Whereas Houk and Praphairaksit³⁷ measured the water load as trapped water vapor, the liquid sample uptake into the plasma was used in this work, which was determined from the difference in solution uptake and spray chamber drain. Based on these findings, the N_2 plasma appears to have a gas temperature that is in the range of ~ 5000 – 6000 K and is thus comparable to an Ar ICP.

Calcium matrix tolerance

The tolerance of the N_2 MICAP-MS against a calcium matrix was investigated, since Ca is a common major matrix element in environmental water samples such as the studied reference materials. Therefore, multi-element solutions with increasing amounts of Ca were measured and the signal suppression was determined with and without aerosol desolvation (Fig. 1 and Table S4†).

As shown in Fig. 1a, the effect of the calcium matrix is noticeable in both cases but more pronounced for the desolvated aerosol. While the signal suppression of lighter elements is more pronounced (up to 30% and 70% for SN and Des, respectively), heavier elements and elements with higher IE exhibit the lowest signal decrease (see Table S4†). The former is most likely due to space charge effects, but the latter cannot be explained entirely. The fact that less suppression was observed for high IE elements would indicate that the ionization suppression by NO is reduced by a decreased water load in the plasma. For the remaining elements, greater suppression was observed. However, this suggests a greater loss of aerosol in the desolvation unit. The observed signal suppression without

aerosol desolvation is similar to that reported for a sodium¹⁰ or iron matrix.²⁴

The use of an internal standard of similar m/z was found to generally reduce this matrix effect. Elements of low m/z such as Li cannot be corrected using In as an internal standard. For aerosol desolvation, 7Li exhibited a signal suppression of 72% without normalization to the internal standard and a 41% suppression with internal standard correction at 100 mg kg^{-1} . However, heavier isotopes deviated by less than 12% with solution nebulization (see Fig. 1b).

Fig. 2 shows the signal enhancement for the desolvated aerosol in samples with different amounts of calcium. While the signal intensity increased by a factor of 10–15 for a mass fraction up to 10 mg kg^{-1} Ca, the enhancement factor is approximately 5 for 100 mg kg^{-1} Ca. The abundance normalized sensitivities obtained with N_2 MICAP-MS are listed in Table S5† for selected elements.

In contrast to all the other elements investigated, boron was suppressed by up to a factor of seven when aerosol desolvation was used. At the same time, the effect of the Ca matrix on B without aerosol desolvation was very similar to Be (suppression by 7% at 100 mg kg^{-1} Ca), while it caused an increase in B sensitivity with aerosol desolvation (increase by 165%, see Table S4†). Spectra of solutions with increasing boron concentration did not reveal the occurrence of boron-containing molecular ions and thus boron is assumed to be lost in the desolvation unit due to its high volatility.⁴³ Jakubowski *et al.*²⁸ suggested that boron in a dry aerosol is more adsorbed at the walls of the sample introduction system than in a wet aerosol. Furthermore, they observed elevated boron concentrations in the desolvation system drain.

It is important to note, that the attainable LODs for the desolvated aerosol are not only improved by the signal enhancement, because the abundance of spectral interferences is reduced as well (*e.g.* $^{40}Ca^{16}O^{16}H^+$ vs. $^{57}Fe^+$ or $^{14}N^{16}O_2^+$ vs. $^{46}Ti^+$). Memory effects in the desolvation system, however, usually lead to elevated background signals for a blank sample and the LODs for a desolvated aerosol in most cases did not improve by the

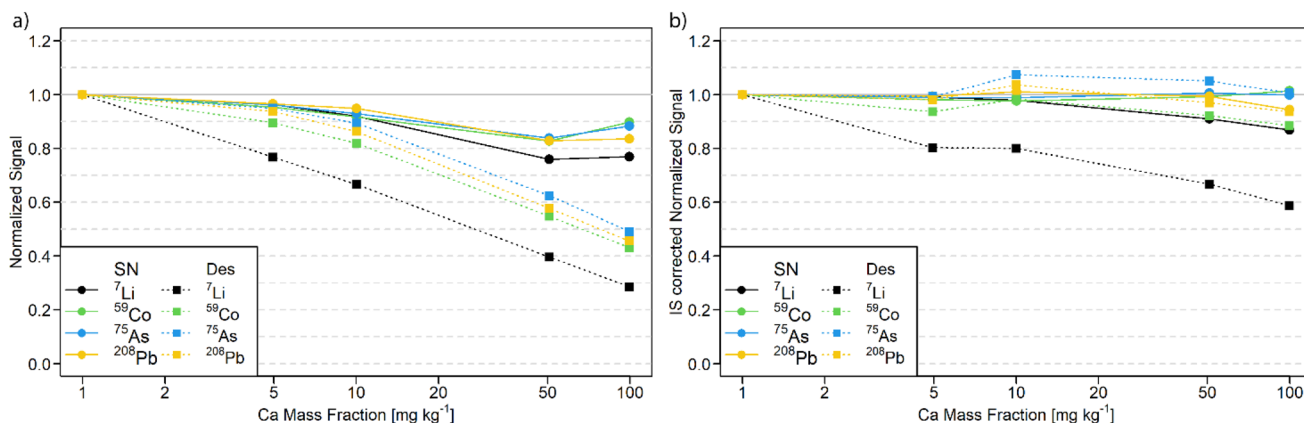


Fig. 1 (a) Observed signal suppression for solution nebulization (solid line with circles) and aerosol desolvation (dotted line with squares) for multi-element solutions with increasing Ca matrix. (b) Employing a correction with the internal standard can reduce the observed signal suppression.



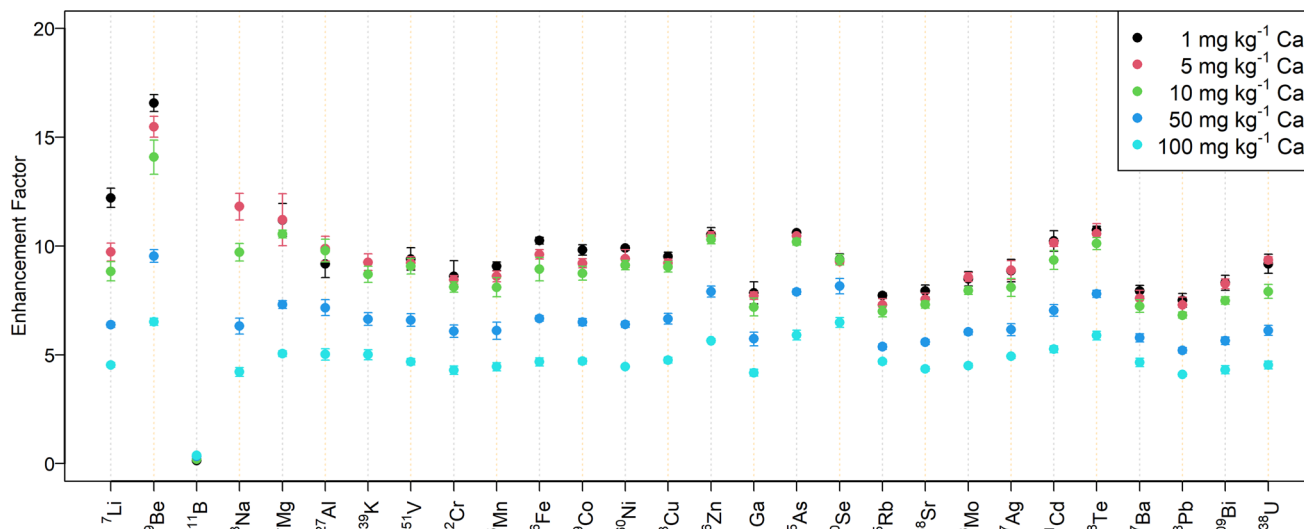


Fig. 2 Signal intensity enhancement of elements contained in a 1000-fold diluted Merck VI standard solution at different calcium amounts. The enhancement corresponds to the factor to which the signals with aerosol desolvation increased.

same factor as the sensitivity enhancement (Table S6†). While a higher signal-to-noise ratio for the desolvated aerosol results in lower detection limits for most elements, the loss of boron in the desolvation unit increased the LOD significantly.

Quantitative analyses using N₂ MICAP-MS

Mass fractions for all elements were determined and, to account for possible spectral interferences, some elements were quantified using multiple isotopes, *e.g.* ⁵⁶Fe and ⁵⁷Fe. Since plasma-based background ions occur predominantly at *m/z* 14–19, *m/z* 28–34, *m/z* 42–46, and *m/z* 56–58, and Ar-based molecular ions

were not detected, the most abundant isotopes could be used for most elements. However, residual Ar in the nitrogen gas occurring at *m/z* 40 and not identified ions at *m/z* 80, *m/z* 82, *m/z* 108, and *m/z* 110,²⁰ were found to affect the signal-to-background ratios attainable for Ca and Se in particular.

Quantitative analyses using solution nebulization

The relative deviations of the mass fractions determined in a twofold diluted NIST SRM 1643f to the reference values are shown in Fig. 3 for external calibration and in Fig. 4 when using standard additions. The corresponding mass fractions are

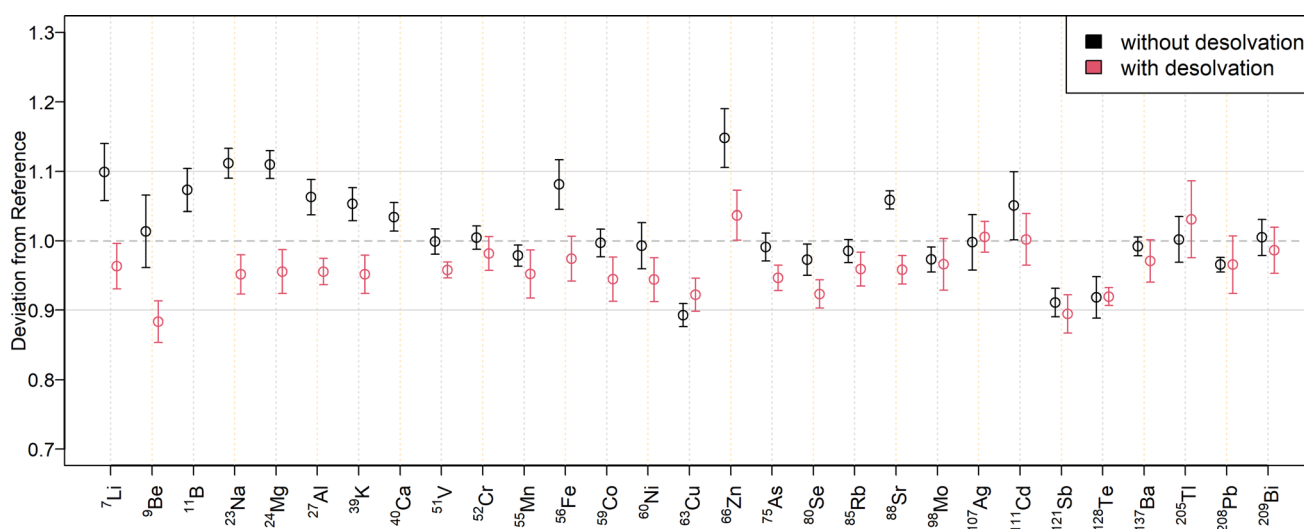


Fig. 3 Quantification overview obtained with a twofold dilution of NIST 1643f for solution nebulization (black circles) and aerosol desolvation (red circles) using external calibration. For each isotope, the deviation of the obtained mass fractions from the certified reference material is given with error bars representing two times the standard deviation. The grey horizontal lines correspond to a difference of $\pm 10\%$ from the certified value. With aerosol desolvation, the boron mass fraction was overestimated by 88%, whereas the ⁴⁰Ca signal exceeded the dynamic range and could not be determined.



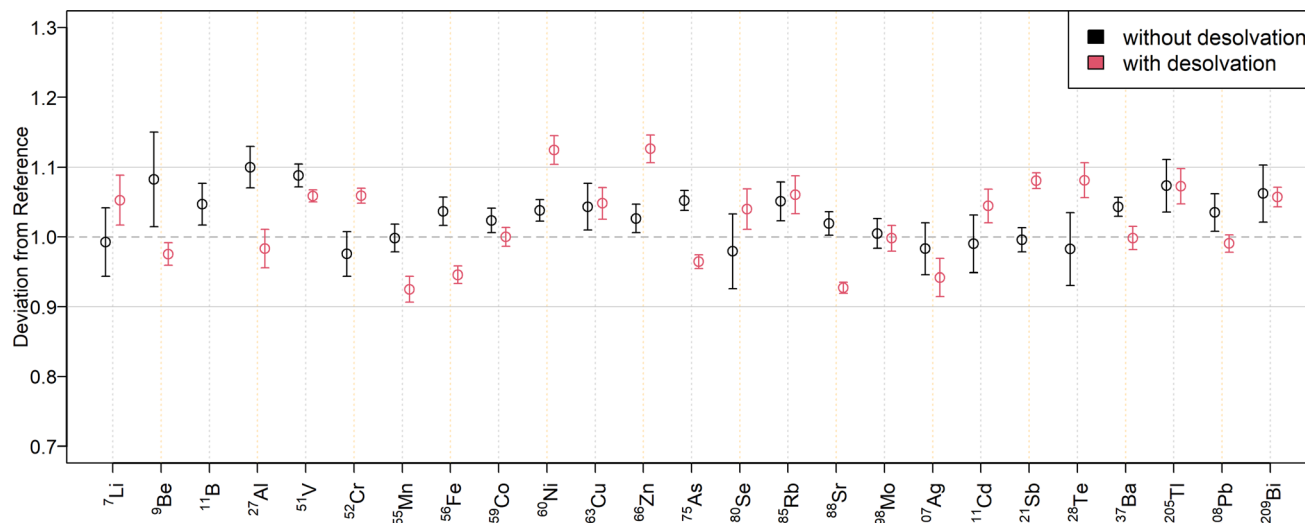


Fig. 4 Quantification overview obtained with a twofold dilution of NIST 1643f for solution nebulization (black circles) and aerosol desolvation (red circles) using standard addition. For each isotope, the deviation of the obtained mass fractions from the certified reference material is given with error bars representing two times the standard deviation. The grey horizontal lines correspond to a difference of $\pm 10\%$ from the certified value. With aerosol desolvation, the boron mass fraction was underestimated by 48%.

listed in Table S7† for all measured isotopes. As can be seen in Fig. 3, most results for SN are within a range of $\pm 10\%$ to the reference values. Only ^{23}Na , ^{24}Mg , and ^{63}Cu deviated by $\pm 11\%$, while ^{64}Zn and ^{66}Zn deviated by $+16\%$ and $+15\%$, respectively. Mass fractions obtained by standard addition (Fig. 4) were all within a $\pm 10\%$ range of the reference values. The higher deviation of the matrix elements may be because they were determined at the upper end of the calibration curve, since the determination with the tenfold dilution of NIST SRM 1643f (Table S8†) resulted in lower deviations. The mass fractions measured in the SLRS-6 reference material were found to match the certified values (Table 3 or Fig. S3 and S4†). Values were typically found within a range of $\pm 10\%$ of the certified values, except for ^{63}Cu , which deviated by -12% when determined by standard addition. While the mass fraction of iron in SLRS-6 was quantified successfully on both ^{56}Fe and ^{57}Fe , the mass fraction in NIST SRM 1643f was overestimated when employing ^{57}Fe regardless of the quantification method (external calibration or standard addition). This difference between the two reference standards can be explained by the approx. three times higher Ca/Fe mass fractions in NIST SRM 1643f compared to SLRS-6 ($29\,140\ \mu\text{g kg}^{-1}/92.51\ \mu\text{g kg}^{-1}$ vs. $8770\ \mu\text{g kg}^{-1}/84.5\ \mu\text{g kg}^{-1}$). This results in a higher abundance of $^{40}\text{Ca}^{16}\text{O}^1\text{H}^+$, which interferes in the determination of iron on ^{57}Fe . In addition to the elements with a certified value, the mass fractions of Li, B, Co, Rb, and Tl were determined in SLRS-6 (Table 3) and U was quantified in NIST SRM 1643f (Tables S7 and S8†). However, the mass fractions of Be, Se, Ag, Cd, Te, and Bi were below their respective LOQ (Table S6†) in SLRS-6 and could thus not be quantified.

Quantitative analyses using aerosol desolvation

To compare the quantification capabilities of the N_2 MICAP-MS when using aerosol desolvation, Fig. 3 depicts the relative

deviations of the determined mass fractions in the twofold dilution of NIST SRM 1643f to the reference values for external calibration, while Fig. 4 shows the relative deviations obtained with standard addition. The determined mass fractions can be found in Table S7† for all isotopes. As can be seen in Fig. 3, all isotopes were quantified with a maximum deviation of $\pm 10\%$ of the certified reference values, except ^{11}B , which was overestimated by 88%, and ^9Be , and ^{121}Sb , which were underestimated by 12% and 11%, respectively. The mass fractions obtained with aerosol desolvation and standard addition (Fig. 4) were mostly in agreement with the reference values, only ^{11}B was underestimated by 48%, while ^{60}Ni (12%), ^{64}Zn (17%) and ^{66}Zn (13%) were overestimated. The mass fraction of ^{40}Ca could not be determined in the twofold dilution, because the ion signal exceeded the dynamic range of the detector (10^9 cps). However, the obtained mass fraction from the tenfold dilution could be accurately determined. As already mentioned in the matrix tolerance section, the boron sensitivity decreased with aerosol desolvation, since boron was lost in the desolvator. The determined mass fractions for SLRS-6 with aerosol desolvation were all within a $\pm 10\%$ range of the certified values, except for ^{238}U , which deviated by -12% when determined by standard addition.

When comparing the quantification with and without aerosol desolvation it can be seen that both trueness and precision are similar. In both SN and Des N_2 MICAP-MS, the obtained mass fractions are within a range of $\pm 12\%$ to the reference values, with only ^{64}Zn and ^{66}Zn varying by $+15\%$ and $+16\%$ for SN using external calibration and by $+17\%$ and $+13\%$ for Des using standard addition with the twofold diluted NIST SRM 1643f reference material. With the tenfold dilution, these deviations decreased and were all lower than 10%, except for ^{64}Zn with Des and standard addition, which decreased from $+17\%$ to $+13\%$. For SLRS-6, the deviations of Zn are all within



Table 3 Quantification overview for SLRS-6 for both external calibration and standard addition using conventional solution nebulization (SN) and desolvated sample introduction (Des). All values are reported in $\mu\text{g kg}^{-1}$. The mass fractions of Be, Se, Ag, Cd, Te, and Bi were below their respective LOQ in all setups and could thus not be quantified

Quantified isotope	Reference		SN ext. cal.		SN std. add.		Des ext. cal		Des std. add.	
	Mean	2SD	Mean	2SD	Mean	2SD	Mean	2SD	Mean	2SD
⁷ Li	0.53 ^a		— ^c		— ^c		0.54	0.06	0.47	0.05
¹¹ B	7.39 ^a		7.8	0.4	5.69	0.20	— ^c		— ^c	
²³ Na	2770	220	2860	60	— ^d		2610	90	— ^d	
²⁴ Mg	2140	60	2250	30	— ^d		2050	50	— ^d	
²⁵ Mg	2140	60	2260	50	— ^d		2060	70	— ^d	
²⁷ Al	33.9	2.2	33.6	0.6	32.5	0.8	31.9	0.3	33.3	0.4
³⁹ K	650	50	670	12	— ^d		614	14	— ^d	
⁴⁰ Ca	8770	200	8710	130	— ^d		8700	160	— ^d	
⁴¹ K	650	50	648	10	— ^d		620	30	— ^d	
⁵¹ V	0.352	0.006	0.351	0.024	0.362	0.016	0.361	0.014	0.351	0.008
⁵² Cr	0.252	0.012	0.255	0.012	0.234	0.012	0.249	0.005	0.236	0.008
⁵³ Cr	0.252	0.012	0.24	0.04	0.24	0.05	0.251	0.020	0.227	0.008
⁵⁵ Mn	2.12	0.10	2.13	0.06	1.972	0.014	2.10	0.08	1.93	0.06
⁵⁶ Fe	85	4	84.1	1.8	82.5	1.4	81	3	78.1	2.6
⁵⁷ Fe	85	4	86.0	1.6	86.7	1.0	90	6	87.5	2.6
⁵⁹ Co	0.053 ^b	0.012	0.074	0.012	0.072	0.002	0.065	0.006	0.057	0.004
⁶⁰ Ni	0.617	0.022	0.59	0.05	0.66	0.02	0.64	0.03	0.676	0.024
⁶² Ni	0.617	0.022	0.58	0.16	0.61	0.04	0.63	0.03	0.61	0.03
⁶³ Cu	24.0	1.8	22.5	0.3	22.0	0.4	24.1	0.6	22.3	0.6
⁶⁴ Zn	1.76	0.12	1.84	0.12	1.85	0.10	1.73	0.12	1.84	0.10
⁶⁵ Cu	24.0	1.8	22.8	0.3	21.17	0.22	23.8	0.8	21.6	0.6
⁶⁶ Zn	1.76	0.12	1.81	0.14	1.85	0.05	1.75	0.12	1.83	0.14
⁷⁵ As	0.57	0.08	0.57	0.03	0.51	0.04	0.53	0.03	0.518	0.026
⁸⁵ Rb	1.41 ^a		1.41	0.05	1.34	0.03	1.43	0.03	1.280	0.016
⁸⁸ Sr	40.7	0.3	37.2	0.6	38.8	0.4	37.5	1.2	38.7	0.8
⁹⁵ Mo	0.215	0.018	0.296	0.015	0.208	0.014	0.201	0.008	0.196	0.006
⁹⁸ Mo	0.215	0.018	0.198	0.022	0.194	0.016	0.198	0.012	0.192	0.010
¹²¹ Sb	0.338	0.006	0.357	0.016	0.314	0.014	0.354	0.020	0.308	0.014
¹³⁷ Ba	14.3	0.5	14.4	0.4	13.4	0.4	14.5	0.4	13.2	0.5
¹³⁸ Ba	14.3	0.5	14.9	0.4	13.8	0.5	14.2	0.8	13.4	0.6
²⁰⁵ Tl	0.0085 ^a		0.0093	0.0018	— ^c		0.0062	0.0005	0.0067	0.0014
²⁰⁸ Pb	0.170	0.026	0.163	0.014	0.165	0.006	0.161	0.014	0.154	0.005
²³⁸ U	0.070	0.003	0.0686	0.0024	0.073	0.004	0.070	0.003	0.0615	0.0012

^a From GeoReM database.⁴⁴ ^b Not certified. ^c Below LOQ. ^d Not determined.

a range of $\pm 5\%$ to the reference values. However, as already mentioned, the determination of boron with aerosol desolvation did not yield accurate values and thus cannot be recommended. The precision of external calibration and standard addition as well as with and without aerosol desolvation was found to be similar, which is also because the errors were estimated from the standard deviations of the diluted certified reference solutions.

Conclusions

The plasma gas temperature of the nitrogen-sustained microwave inductively coupled atmospheric pressure plasma was calculated with three different methods. The values at the optimized operating conditions for conventional solution nebulization and desolvated sample introduction were found to be very similar. In addition, the values for the N_2 MICAP were found to be in good agreement with gas temperatures reported for an Ar ICP, indicating that the plasma gas temperature is not

substantially different. For a typical optimization, the temperature was found to be in the range of ~ 5000 – 6000 K regardless of the plasma gas or the sample introduction method.

The presence of a calcium matrix resulted in moderate suppression of the analyte sensitivities up to 30% when aspirating solutions of up to 100 mg kg^{-1} Ca with solution nebulization or 70% with aerosol desolvation. Indium was found to be a suitable internal standard for most elements investigated and compensated matrix effects for up to 100 mg kg^{-1} of Ca. The exception (Li) would require the use of an additional internal standard. Using aerosol desolvation can be beneficial due to the observed signal enhancement and lower limits of detection. However, matrix effects and possible analyte losses in the desolvator need to be considered.

The quantitative analyses of NIST 1643f and SLRS-6 have shown that using the nitrogen plasma source for inorganic mass spectrometry, the mass fractions of 30 elements could be determined. The most abundant isotopes of potassium, calcium, chromium, iron, and selenium could be used for their



quantification. Since the obtained mass fractions from external calibration and standard addition are in good agreement, no substantial matrix effect was observed for the water reference materials. The trueness and precision using external calibration and standard addition as well as with and without aerosol desolvation were found to be similar. These results show that SN N₂ MICAP-MS can be used as a more economic, competitive, or complementary instrument to Ar ICP-MS for routine analysis.

Author contributions

Monique Kuonen investigation, formal analysis, writing – original draft. Bodo Hattendorf supervision, writing – review & editing. Detlef Günther conceptualization, funding acquisition, supervision, writing – review & editing.

Conflicts of interest

The authors have neither financial nor personal conflicts of interest to declare.

Acknowledgements

The authors acknowledge the technical support from Ashok Menon and Jovan Jevtic of Radom Corporation, the assistance from the D-CHAB central and electronic workshop through Philippe Trüssel and Tiago Ferreira des Neves respectively, the help from the D-PHYS laboratory support group and the financial support from the Swiss National Science Foundation (project number 200021_197224).

References

- J. Jevtic, A. Menon and V. Pikelja, *US Pat.*, PCT/US2014/024306, 2014.
- C. I. M. Beenakker, *Spectrochim. Acta, Part B*, 1976, **31**, 483–486.
- J. Hubert, M. Moisan and A. Ricard, *Spectrochim. Acta, Part B*, 1979, **34**, 1–10.
- Q. Jin, C. Zhu, M. W. Borer and G. M. Hieftje, *Spectrochim. Acta, Part B*, 1991, **46**, 417–430.
- Y. Okamoto, M. Yasuda and S. Murayama, *Jpn. J. Appl. Phys.*, 1990, **29**, L670–L672.
- Y. Okamoto, *J. Anal. At. Spectrom.*, 1994, **9**, 745–749.
- D. Potter, *J. Anal. At. Spectrom.*, 2008, **23**, 690–693.
- K. J. Jankowski and E. Reszke, *Encyclopedia of Analytical Chemistry*, 2023, pp. 1–80.
- A. J. Schwartz, Y. Cheung, J. Jevtic, V. Pikelja, A. Menon, S. J. Ray and G. M. Hieftje, *J. Anal. At. Spectrom.*, 2016, **31**, 440–449.
- M. Schild, A. Gundlach-Graham, A. Menon, J. Jevtic, V. Pikelja, M. Tanner, B. Hattendorf and D. Günther, *Anal. Chem.*, 2018, **90**, 13443–13450.
- S. Greenfield, I. L. Jones, C. T. Berry and J. M. Mermet, *J. Anal. At. Spectrom.*, 1964, **4**, 559–560.
- R. H. Wendt and V. A. Fassel, *Anal. Chem.*, 1965, **37**, 920–922.
- R. S. Houk, *Anal. Chem.*, 1980, **52**, 2283–2289.
- W.-L. Shen, T. M. Davidson, J. T. Creed and J. A. Caruso, *Appl. Spectrosc.*, 1990, **44**, 1003–1010.
- M. C. Lomax-Vogt, F. Liu and J. W. Olesik, *Spectrochim. Acta, Part B*, 2021, **179**, 106098.
- I. Feldmann, N. Jakubowski and D. Stuewer, *Fresenius. J. Anal. Chem.*, 1999, **365**, 415–421.
- S. D. Tanner and V. I. Baranov, *J. Am. Soc. Mass Spectrom.*, 1999, **10**, 1083–1094.
- B. Hattendorf and D. Günther, *J. Anal. At. Spectrom.*, 2000, **15**, 1125–1131.
- I. Feldmann, W. Tittes, N. Jakubowski, D. Stuewer and U. Giessmann, *J. Anal. At. Spectrom.*, 1994, **9**, 1007–1014.
- C. Neff, P. Becker, B. Hattendorf and D. Günther, *J. Anal. At. Spectrom.*, 2021, **36**, 1750–1757.
- M. R. Hammer, *Spectrochim. Acta, Part B*, 2008, **63**, 456–464.
- K. M. Thaler, A. J. Schwartz, C. Haisch, R. Niessner and G. M. Hieftje, *Talanta*, 2018, **180**, 25–31.
- F. Hallwirth, M. Wolfgang and H. Wiltsche, *J. Anal. At. Spectrom.*, 2023, **38**, 1682–1690.
- A. Winkelmann, J. Roik, S. Recknagel, C. Abad and Z. You, *J. Anal. At. Spectrom.*, 2023, **38**, 1253–1260.
- R. C. Hutton and A. N. Eaton, *J. Anal. At. Spectrom.*, 1987, **2**, 595–598.
- S. E. Long and R. F. Browner, *Spectrochim. Acta*, 1988, **43**, 1471.
- R. Tsukahara and M. Kubota, *Spectrochim. Acta, Part B*, 1990, **45**, 581–589.
- N. Jakubowski, I. Feldmann and D. Stuewer, *Spectrochim. Acta, Part B*, 1992, **47**, 107–118.
- P. W. J. M. Boumans and F. J. de Boer, *Spectrochim. Acta, Part B*, 1976, **31**, 355–375.
- L. Halicz and D. Günther, *J. Anal. At. Spectrom.*, 2004, **19**, 1539–1545.
- M. Kuonen, G. Niu, B. Hattendorf and D. Günther, *J. Anal. At. Spectrom.*, 2023, **38**, 758–765.
- R. Serrano, G. Grindlay, L. Gras and J. Mora, *Talanta*, 2024, **271**, 125666.
- S. Mukta and A. Gundlach-Graham, *J. Anal. At. Spectrom.*, 2024, **39**, 491–499.
- Z. You, A. Akkuş, W. Weisheit, T. Giray, S. Penk, S. Buttler, S. Recknagel and C. Abad, *J. Anal. At. Spectrom.*, 2022, **37**, 2556–2562.
- J. E. Fulford and D. J. Douglas, *Appl. Spectrosc.*, 1986, **40**, 971–974.
- H. P. Longerich, *J. Anal. At. Spectrom.*, 1989, **4**, 491–497.
- R. S. Houk and N. Praphairaksit, *Spectrochim. Acta, Part B*, 2001, **56**, 1069–1096.
- CRC Handbook of Chemistry and Physics*, ed. J. Rumble, CRC Press, Boca Raton, FL, 104th edn, 2023.
- M. Kubota, N. Fudagawa and A. Kawase, *Anal. Sci.*, 1989, **5**, 701–706.
- N. Shibata, N. Fudagawa and M. Kubota, *Spectrochim. Acta, Part B*, 1993, **48**, 1127–1137.
- H. Niu and R. S. Houk, *Spectrochim. Acta, Part B*, 1996, **51**, 779–815.
- NIST Chemistry WebBook*, NIST Standard Reference Database Number 69, ed. P. J. Linstrom and W. G. Mallard, National



Paper

- Institute of Standards and Technology, Gaithersburg MD, 20899, 2021.
- 43 M. V. Stackelberg, F. Quatram and J. Dressel, *Zeitschrift für Elektrochemie und Angew. Phys. Chemie*, 1937, **43**, 14–28.
- 44 K. P. Jochum, U. Nohl, K. Herwig, E. Lammel, B. Stoll and A. W. Hofmann, *Geostand. Geoanal. Res.*, 2005, **29**, 333–338.

